IET Microwaves, Antennas & Propagation

Research Article

IET Journals
The Institution of Engineering and Technology

Beam-forming capabilities of a plasma circular reflector antenna

ISSN 1751-8725
Received on 11th January 2018
Revised 7th June 2018
Accepted on 23rd July 2018
E-First on 2nd October 2018
doi: 10.1049/iet-map.2018.5178
www.ietdl.org

Davide Melazzi[1] ✉, Paola De Carlo[2], Fabio Trezzolani[1], Marco Manente[1], Antonio-Daniele Capobianco[3], Stefano Boscolo[4]

[1]*T4i S.r.l, via della Croce Rossa 112, 35129 Padova, Italy*
[2]*Center of Studies and Activities for Space 'G.Colombo', Università degli Studi di Padova, via Venezia 15, 35131 Padova, Italy*
[3]*Dipartimento di Ingegneria dell'Informazione, Università degli Studi di Padova, via Gradenigo 6/b, 35131 Padova, Italy*
[4]*Dipartimento Politecnico di Ingegneria e Architettura, Università degli Studi di Udine, via delle Scienze 206, 33100 Udine, Italy*
✉ *E-mail: davide.melazzi@gmail.com*

Abstract: A gaseous plasma antenna array (PAA) is an aggregate of plasma discharges and possibly conventional metallic radiating elements, and it constitutes a promising alternative to metallic antennas for applications in which fast reconfiguration of radiation pattern, and gain is desired; such properties can be achieved by exploiting the electronic switch on/off condition of plasma discharges, and tuning of the plasma parameters. Here, the authors present a reconfigurable PAA that features a central metallic half-wavelength dipole working around 1.45 GHz, surrounded by a planar circular lattice of cylindrical plasma discharges. Customised plasma discharges have been realised, and filled with argon gas at 2 mbar so as to have a complete control on the plasma discharge properties (e.g. plasma frequency, collisional frequency). The magnitude of the reflection coefficient, and the gain pattern on the *H*-plane have been investigated numerically and experimentally; numerical and experimental results exhibit a good agreement and show that the central intrinsically omnidirectional antenna can provide simple beamforming capabilities upon turning on a subset of plasma discharges; as these plasma discharges are turned on, the authors have observed a maximum gain of ∼5 dBi, a half-power beam width of 80°, and an angular steering resolution of ∼15°.

1 Introduction

Plasma antennas have been broadly defined as devices that exploit plasma discharges and metallic structures to transmit and receive electromagnetic (EM) waves similarly to a traditional antenna [1]; the distinctive trait of these antennas is the use of a weakly or fully ionised plasma as conductive medium [2]. Specifically, a single plasma discharge confined in a dielectric tube can be used as an active element to build a gaseous plasma antenna (GPA), which will have a proper radiation pattern when the plasma discharge is turned 'on' and the antenna is driven at a frequency smaller than the plasma frequency [3]. It has been demonstrated that the performance of a GPA is equivalent to that of a metallic counterpart in every respect [4]; however, it can also offer several advantages such as electronically reconfigurable with respect to frequency, and gain on time scales the order of microseconds to milliseconds [5], and being transparent to incoming EM waves whose frequency is greater than the plasma frequency. Conversely, when the plasma is 'off', the GPA reverts to a dielectric tube with a very low radar cross-section, thus making such antennas appealing for stealth communications.

A plasma antenna array (PAA) can be realised by either stacking GPAs of different type, or combining plasma discharges that act as passive antenna elements with conventional metallic elements; this approach allows PAAs to have the above-mentioned advantages of GPAs; however, it allows them to steer the beam in the direction of interest, to improve the directivity by adding nulls to the radiation pattern and to afford multi-beam operation. These characteristics can be further exploited in smart plasma antennas (SPA), in which a PAA endowed with smart signal processing algorithms allows (i) identifying the direction of an incoming signal, (ii) tracking and locating the antenna beam on a mobile target, and (iii) steering the beam in the direction of interest while minimising interferences [6]. In conventional antenna arrays, the direction and the width of the main lobe is mainly determined by the relative positions of the elements, the amplitude and progressive phase difference of the excitation of the elements, and the resulting radiation pattern. In addition, the PAA radiation pattern is controlled by the complex dielectric permittivity of the plasma that depends on the wave frequency (ω), the plasma density (n_0), and the neutral background pressure (pn) if the plasma is weakly ionised [7]. Since numerical models have proven particularly useful to grasp the underlying physics, and to assess the effect of plasma macroscopic parameters (e.g. plasma density) on the radiation properties of PAAs [8], different groups have reported the radiation properties of several PAAs configurations, namely: (i) the beam-forming and multi-beam operations of an omnidirectional radiating element that is surrounded by up to 20 plasma discharges [9]; (ii) the reconfiguration capabilities of an array of monopole GPAs [10]; (iii) the beam-shaping and beam-scanning properties of a plasma reflectarray [8] (transmitarray [11]) that relies on a planar layer of plasma discharges to reflect (transmit) the incident fields radiating from a feed antenna.

From a technology standpoint, a plasma discharge confined in a dielectric tube (e.g. glass) may come in different shapes (e.g. loops), we can rely on different methods to generate the plasma discharge, like laser-initiated atmospheric discharge [12], DC/AC discharges [13], radio-frequency surface-wave plasmas [14], and pulsed power technique [2]. The efficiency of the plasma generation method differs (i.e. plasma density reached with a given power consumption), and can introduce noise; as a result, the ultimate choice in terms of plasma discharge shape and generation system is driven by the intended application. So far, experimental works have reported (i) on the generation of a plasma mirror for microwave beam steering [15–17], and (ii) on the beam-forming capabilities of PAAs with a central radiating monopole surrounded by plasma discharges that are arranged in a circular [18], square [19], and corner-shaped [20] arrangements. In the above-mentioned PAA prototypes, the plasma discharges have been made from fluorescent lamps because they are inexpensive, and no knowledge of plasma discharge technology is required; unfortunately, this approach allows to build prototypes with the discharge dimensions that are available on the market, and, more importantly, no

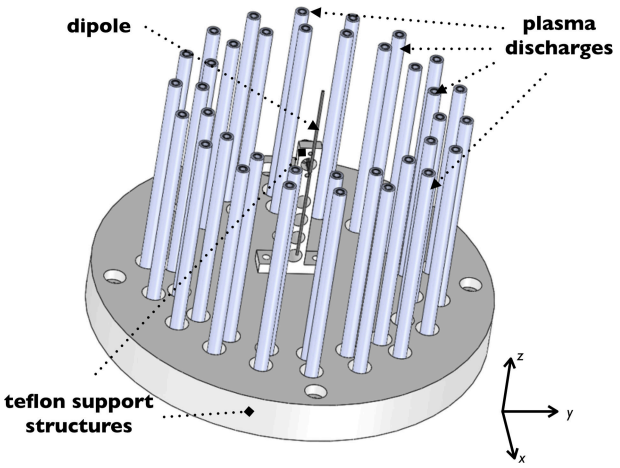

Fig. 1 *Model of the PAA composed of a central metallic half-wavelength, 36 plasma discharges, and Teflon supports*

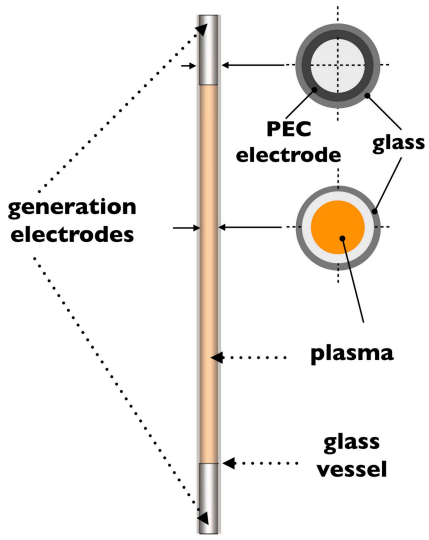

Fig. 2 *Detailed view of the model of the plasma discharges that are composed of the cylindrical plasma region, two PEC generation electrodes, and a glass confinement vessel*

information about the gas mixtures and partial pressures can be inferred, thus preventing any self-consistent analysis of the PAA performance.

In this work, we present the numerical and experimental characterisation of a PAA that has been specifically built for the Galileo navigation frequency band, i.e. from 1.164 GHz up to 1.592 GHz. The PAA prototype comprises an intrinsically omnidirectional antenna, i.e. a dipole that works in the previously mentioned frequency band, with a set of plasma discharges; the resulting device is an electronically reconfigurable antenna that allows for beam-forming operations by selectively switching on and off the plasma discharges. Besides, such discharges have been realised with customised dimensions, filled with argon gas at a prescribed pressure, and whose plasma density has been measured by means of a microwave interferometer; using this approach, we can uniquely determine the plasma electric permittivity for a self-consistent numerical characterisation of the PAA performance, which has been performed by means of a well-established integral equation solver [21]. The rest of this paper is organised as follows, Section 2 presents the antenna design and the expected reconfigurable properties, with the antenna prototype description and the plasma density measurements shown in Section 3. In Section 4, we discuss the numerical and experimental results regarding antenna parameters, and radiation properties; finally, conclusions are drawn in Section 5.

2 Antenna model

In accordance with basic design rules of reflector antennas, which can be accessed from many antenna reference books (e.g. [22]), this section presents the model of a plasma circular reflector antenna in which an array of plasma discharges surrounding a radiating element effectively establishes a reconfigurable plasma reflector. Specifically, the antenna consists of a conventional metallic half-wavelength dipole antenna surrounded by 36 plasma discharges. To work in the band of interest, the dipole is 90 mm long, has a radius of 0.5 mm, and a gap of ∼2 mm; the dipole is placed at the centre of the cluster of discharges, as illustrated in Fig. 1.

The plasma discharge is cylindrically shaped, with a height of 100 mm, and a diameter of 6 mm; the dimensions and shape of the plasma discharges are specifically designed to act as reflectors. Inside the discharge, the plasma is assumed uniform and it is confined in glass tubes (i.e. lossy Pyrex) that are 148 mm long, with an inner diameter that is the same of the plasma discharge, and a wall thickness of ∼1 mm. To allow for a uniform plasma generation we have assumed a capacitive generation technique [13] that relies on two distinct metallic electrodes immersed in the plasma and placed at the far ends of the glass vessels; specifically, the hollow electrodes have a length of 20 mm, an inner and outer radius of 2 and 3 mm, respectively (see Fig. 2). Such dimensions are readily accessible on the market. The discharges are arranged in two concentric circles with a radius of 52 and 60 mm, respectively, based on a preliminary numerical assessment. On each circle, we have placed 18 discharges that are thus placed 20° apart. Note, instead of one discharge for each angular position, the peculiar arrangement of two discharges allows a series connection between the two of them in the PAA prototype, keeps the power supply lines beneath the dipole, and thus minimise any interference on the radiation pattern from stray conductors. To provide structural robustness to the antenna, we have added a cylindrically shaped base, made of lossy Teflon with a diameter of 180 mm, and a height of 20 mm. In addition, 36 through holes have been drilled to allow proper placement of the plasma discharges; specifically, the tubes have been inserted into the holes in such a way that one electrode is wholly contained in the base. Finally, another support of lossy Teflon has been added to keep the dipole aligned with the axis of the discharge assemble; this support has dimensions of $10 \times 5 \times 65$ mm^3, and it has a through hole of 10 mm in diameter, whose axis is ∼10 mm from the top face.

In the PAA model, the plasma inside each discharge has been assumed a weakly ionised plasma in which the thermal motion of the ions is ignored, and the electric field intensity of the EM wave radiated by the central dipole is 'small' enough for the electron density and the spatial distribution to remain temporally constant; therefore, the plasma response can be represented by means of a cold fluid model [23] that results in a medium with relative dielectric permittivity $\epsilon_r = \epsilon/\epsilon_0$

$$\epsilon_r = \left(1 - \frac{\omega_{pe}^2}{\omega^2 + \nu^2}\right) - j\frac{\nu}{\omega}\left(\frac{\omega_{pe}^2}{\omega^2 + \nu^2}\right) \tag{1}$$

where ω is the antenna angular frequency, $\omega_{pe} \equiv \left(n_0 q_e^2/\epsilon_0 m_e\right)^{1/2}$ the plasma frequency, and n_0 the plasma density. All dissipation mechanisms are lumped into one phenomenological collision frequency (ν) that accounts for both charge–charge and charge–neutral collisions (see [23, p. 105]) that depends on the plasma density and neutral gas pressure, respectively. Thanks to the numerical model in Fig. 1, we have identified a plasma density value of $n_0 = 4 \times 10^{18}\text{m}^{-3}$ as a compromise that makes the plasma discharges acting as reflective elements, while being achievable by conventional plasma generation systems (e.g. inductive/capacitive discharges [13]).

2.1 Pattern reconfiguration

The array of plasma discharges surrounding the central dipole effectively shields the unwanted incoming EM waves. Additionally, windows can be opened in suitable positions to let outward EM waves through. As a result, the pattern

reconfiguration, chiefly the beam-forming and beam-scanning operations, is based upon the state (on or off) of the discharges, and the plasma properties thereof as well as the interaction between the plasma window and the incident EM wave.

To uniquely identify the plasma discharges that are on (off), we consider the circle where the discharges are placed and number them counter-clockwise for each angular position (α_j, $j = 1, \ldots, 18$) starting from the two discharges that are along the dipole-Teflon line (see Fig. 3); as a result, each angular position identifies two discharges. Moreover, we have labelled as $\alpha_j = 1$ $(\alpha_j = 0)$ the two discharges that occupy the jth angular position, and that are turned on (off). The operating configurations of the PAA will hence be referred to as '*conf-i*' ($i = 1, \ldots, 20$), see Table 1 for table of configurations. In the first configuration (i.e. *conf-1*), we expect the omnidirectional radiation pattern of the dipole due to the absence of any plasma discharge; conversely, no transmission/reception capabilities on the *H*-plane of the dipole is expected by the last configuration (i.e. *conf-20*) due to the presence of a plasma reflector that shields the dipole. The remaining configurations show plasma discharges that are ignited at nine angular positions (a condition that maximises the gain on the *H*-plane) and allow the main lobe to be steered in 18 directions, namely: 0°, 20°, 40°, 60°, 80°, 100°, 120°, 140°, 160°, 180°, 200°, 220°, 240°, 260°, 280°, 300°, 320°, and 340°.

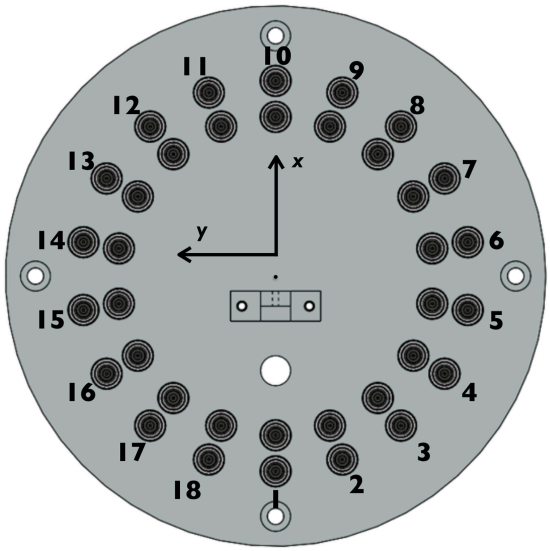

Fig. 3 *Frontal view of the PAA with the numbering of the angular positions*

3 Experimental set-up

We have developed the PAA (see Fig. 4) according to the antenna model of Fig. 1, whose dimensions reflect in the prototype. The Teflon support structure is made of two circular plates; the upper plate is meant to house the plasma discharges and the dipole, which is mounted on a Teflon turret protruding from the centre of the plate. The lower plate is joined to the upper one by means of four Teflon columns to provide mechanical robustness and contains the electrical connectors for the power feed lines. All the elements are fastened together by means of Teflon screws. We resorted on a 50 Ω coaxial cable to feed the dipole.

Each plasma discharge comprises a cylindrical Pyrex vessel, and two cold cathode electrodes with a current rating of 20–30 mA to ignite and sustain the plasma discharge. The two discharges at each angular position have been soldered in series, to avoid any power supply line above the dipole in the effort to keep all the high-voltage cables below the antenna. The power supply for each couple of discharges is an electronic ballast that provides a maximum output voltage of 2 kV at the frequency of ∼19 kHz; besides, each ballast is controlled by a breaker switch that allows for secure activation of the plasma discharges. Finally, we have placed matching capacitors of ∼1.5 nF between the discharges and the power supply in the effort to increase the efficiency in generating plasma, and thus achieve the highest plasma density. Each discharge has been filled with argon at a pressure of 2 mbar (that has been measured by means of an absolute vacuum dial gauge with an accuracy of ±5% in the range 0–25 mbar) that resulted in the target density value for the plasma to exhibit good electrical conductivity, and thus to reflect the fields radiated by the dipole.

3.1 Plasma density measurement

The plasma discharges have been characterised in terms of plasma density. With the aim of mapping the plasma density within the discharges, we relied on a microwave interferometer, which is capable of plasma density measurements regardless of the gas type [24]. The instrument is movable along the axis of the discharge and measures the average electron density in a plasma slab extending to the entire diameter of the source (see Fig. 5). This averaged value of the plasma density is representative of the EM interaction of the

Table 1 Operating configurations of the PAA

configuration	α_1	α_2	α_3	α_4	α_5	α_6	α_7	α_8	α_9	α_{10}	α_{11}	α_{12}	α_{13}	α_{14}	α_{15}	α_{16}	α_{17}	α_{18}
conf-1	0	0	0	0	0	0	0	0	0	0	0	0	0	0	0	0	0	0
conf-2	1	1	1	1	1	1	1	1	1	0	0	0	0	0	0	0	0	0
conf-3	0	1	1	1	1	1	1	1	1	1	0	0	0	0	0	0	0	0
conf-4	0	0	1	1	1	1	1	1	1	1	1	0	0	0	0	0	0	0
conf-5	0	0	0	1	1	1	1	1	1	1	1	1	0	0	0	0	0	0
conf-6	0	0	0	0	1	1	1	1	1	1	1	1	1	0	0	0	0	0
conf-7	0	0	0	0	0	1	1	1	1	1	1	1	1	1	0	0	0	0
conf-8	0	0	0	0	0	0	1	1	1	1	1	1	1	1	1	0	0	0
conf-9	0	0	0	0	0	0	0	1	1	1	1	1	1	1	1	1	0	0
conf-10	0	0	0	0	0	0	0	0	1	1	1	1	1	1	1	1	1	0
conf-11	0	0	0	0	0	0	0	0	0	1	1	1	1	1	1	1	1	1
conf-12	1	0	0	0	0	0	0	0	0	0	1	1	1	1	1	1	1	1
conf-13	1	1	0	0	0	0	0	0	0	0	0	1	1	1	1	1	1	1
conf-14	1	1	1	0	0	0	0	0	0	0	0	0	1	1	1	1	1	1
conf-15	1	1	1	1	0	0	0	0	0	0	0	0	0	1	1	1	1	1
conf-16	1	1	1	1	1	0	0	0	0	0	0	0	0	0	1	1	1	1
conf-17	1	1	1	1	1	1	0	0	0	0	0	0	0	0	0	1	1	1
conf-18	1	1	1	1	1	1	1	0	0	0	0	0	0	0	0	0	1	1
conf-19	1	1	1	1	1	1	1	1	0	0	0	0	0	0	0	0	0	1
conf-20	1	1	1	1	1	1	1	1	1	1	1	1	1	1	1	1	1	1

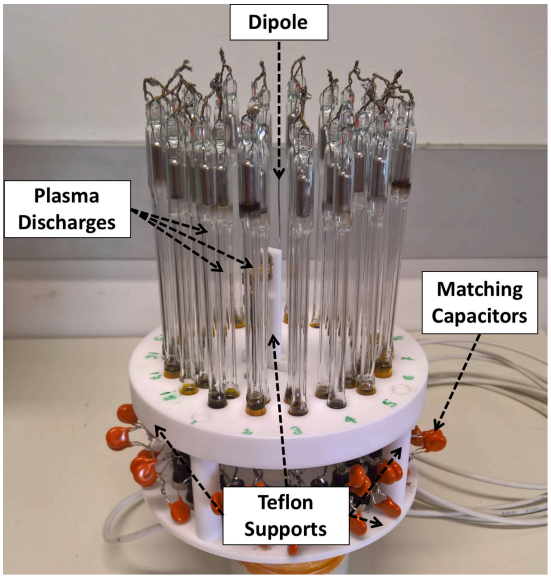

Fig. 4 *PAA prototype*

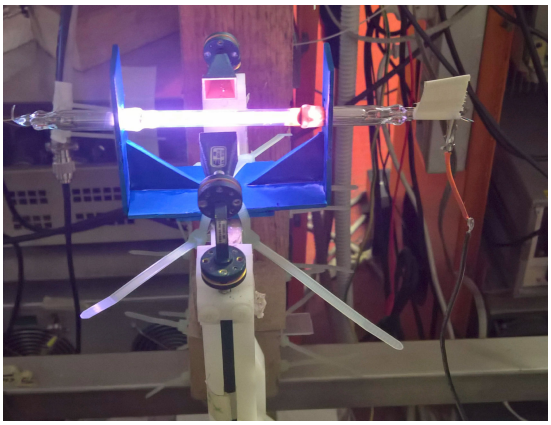

Fig. 5 *Measurement of the plasma density by means of the microwave interferometer [23]*

fields that are radiated by the dipole with the plasma discharges, since the plasma skin depth is given by

$$\delta_{\mathrm{p}} = -\frac{c}{\omega}\Im\left(\epsilon_{\mathrm{r}}^{-1/2}\right) \tag{2}$$

and is comparable to the discharge radius. Furthermore, the device response is linear in the $10^{16} - 7 \times 10^{19}\mathrm{m}^{-3}$ range of plasma density values, and for a value of discharge diameter from 20 mm down to 8 mm; conversely, corrective factors can be estimated for lower values of the diameter by means of ray tracing techniques (see [24]).

We measured the plasma density values at three distinct positions along the discharge axis, at 10, 50, and 90 mm from one end of the discharge, assessing the plasma density error by considering the accuracy in the estimated geometrical parameters (i.e. the discharge diameter, and the measurement section location) and the phase noise of the interferometer. The density values along with the error bars for the two discharges at the angular position $j = 1$ have been reported in Fig. 6, from which we can infer a uniform plasma density along the discharge, and close to the target density value of $4 \times 10^{18}\mathrm{m}^{-3}$; this holds true for all discharges of the prototype. As a result, we estimated a representative mean density value for all discharges (i.e. $n_0 = 4.8 \times 10^{18}\mathrm{m}^{-3}$).

4 Results and discussion

To consider the effect of the actual plasma density within the discharges, we have updated the model of Fig. 1 with representative mean density value by changing accordingly the

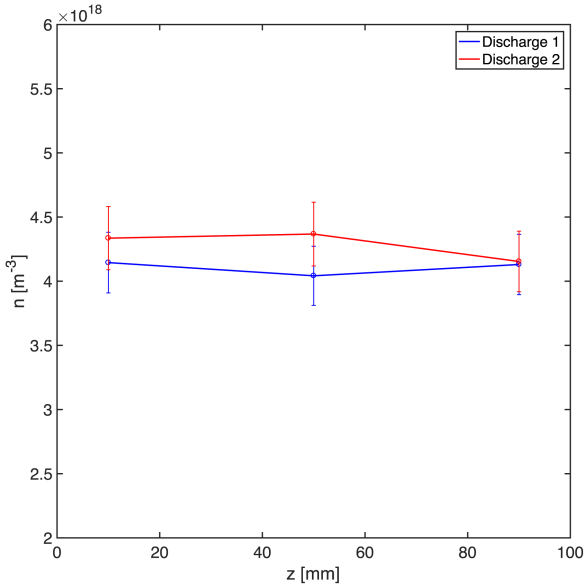

Fig. 6 *Measured plasma density values at three different positions along the axis of the discharge*

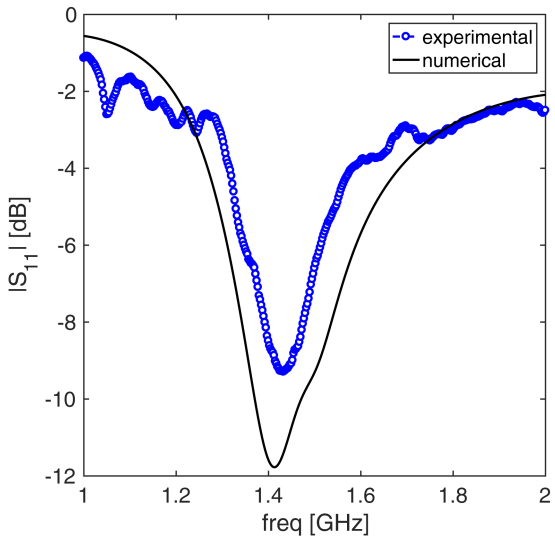

Fig. 7 *Magnitude of the reflection coefficient (reference impedance $Z_0 = 50\,\Omega$) of conf-16 (see Table 1 for table of configurations) from the measurement in the anechoic chamber (experimental), and the simulation (numerical)*

value of the relative electric permittivity of the discharges with the aid of (1); the results from such a model in the range of frequency 1–2 GHz (henceforth referred to as *numerical*) have been compared against the measurements (hereafter referred to as *experimental*) that have been obtained by testing the antenna prototype in an anechoic chamber by means of an Agilent N5230 PNA-L vector network analyser and a wide-band dual-ridge horn, as reference antenna. To begin with, we have reported the magnitude of the reflection coefficient (reference impedance $Z_0 = 50\Omega$) of *conf-16* (see Table 1 for table of configurations) in Fig. 7, in which there is an acceptable correspondence between measurements and simulation results; the discrepancy can be ascribed to (i) the different value of the plasma density that is achieved within each discharge, (ii) the presence of a plasma density profile, though weak, along the axis of the discharge, and (iii) the uncertainty in the filling pressure of the neutral gas. Besides, the minimum of the reflection coefficient is approximately at 1.45 GHz.

Afterwards, we have considered *conf*-16, *conf*-3, *conf*-7, and *conf*-12 (see Table 1 for table of configurations), whose gain patterns on the *H*-plane have been reported in Figs. 8–11, respectively, to prove the PAA capability of scanning the beam

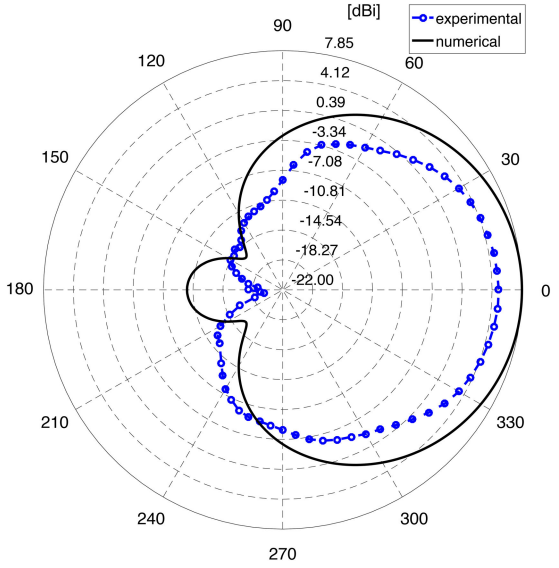

Fig. 8 *Gain pattern ($g(\theta)$ in dBi) on the H-plane at 1.45 GHz from measurement in the anechoic chamber (experimental), and simulation (numerical) of the conf-16 (see Table 1 for table of configurations) of the plasma array antenna. θ angles are measured from x-axis to y-axis (see Fig. 1)*

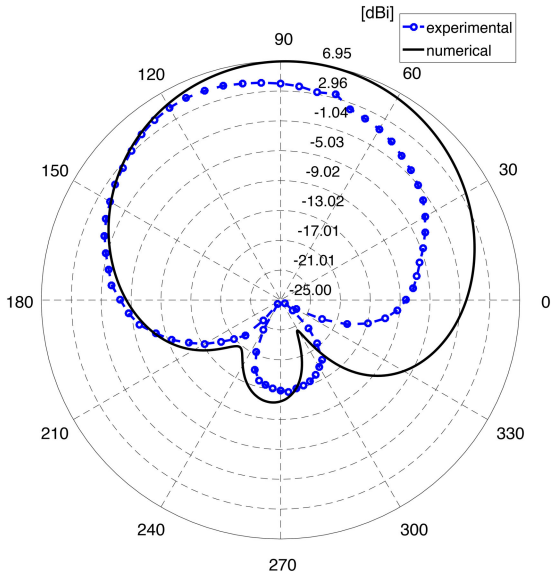

Fig. 9 *Gain pattern ($g(\theta)$ in dBi) on the H-plane at 1.45 GHz from measurement in the anechoic chamber (experimental), and simulation (numerical) of the conf-3 (see Table 1 for table of configurations) of the plasma array antenna. θ angles are measured from x-axis to y-axis (see Fig. 1)*

over 360° on the *H*-plane. The peak gain, the main lobe direction, the half power beam width (HPBW), and the front-to-back (FB) ratio from the measurements in the anechoic chamber have been summarised in Table 2, while the same numerically calculated quantities have been reported in Table 3. The measurements of the radiation pattern exhibit a satisfactory agreement with the numerical results, while there are variations in the peak gain, main lobe direction, HPBW, and FB ratio values that can be attributed to (i) the non-uniform plasma density inside each discharge, (ii) the non-identical value in electric permittivity that is realised in different discharges, and (iii) the complexity of the experimental set-up, which includes the matching network components, high-voltage connectors, and the cables to ignite and sustain the plasma discharges. Despite being lossy, the glass tubes that confine the plasma discharges have a negligible effect, as assessed by numerical simulations.

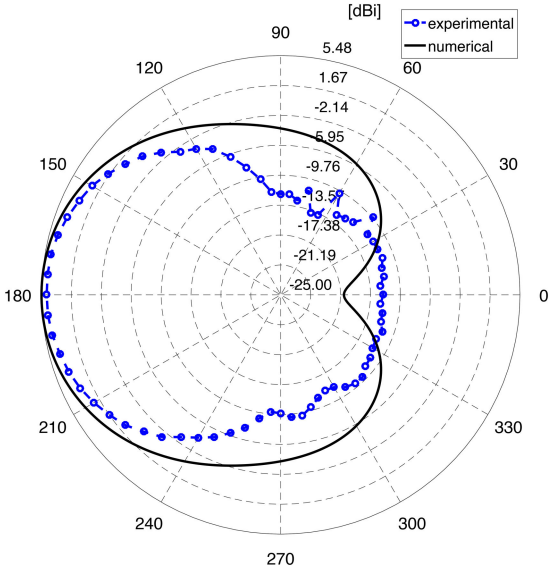

Fig. 10 *Gain pattern ($g(\theta)$ in dBi) on the H-plane at 1.45 GHz from measurement in the anechoic chamber (experimental), and simulation (numerical) of the conf-7 (see Table 1 for table of configurations) of the plasma array antenna. θ angles are measured from x-axis to y-axis (see Fig. 1)*

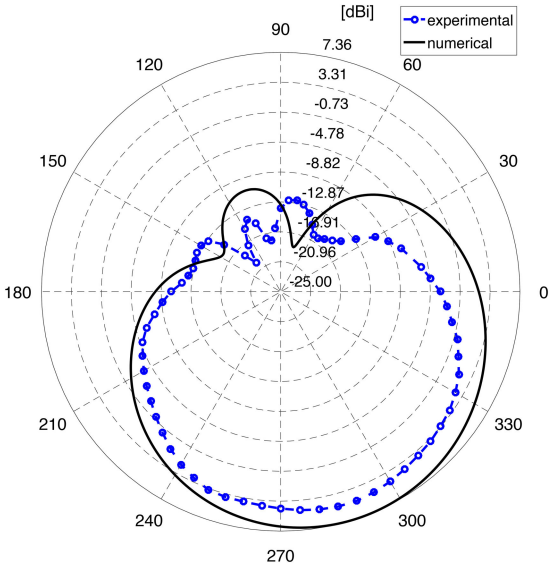

Fig. 11 *Gain pattern ($g(\theta)$ in dBi) on the H-plane at 1.45 GHz from measurement in the anechoic chamber (experimental), and simulation (numerical) of the conf-12 (see Table 1 for table of configurations) of the plasma array antenna. θ angles are measured from x-axis to y-axis (see Fig. 1)*

Table 2 Measured peak gain, main lobe direction, HPBW, and FB ratio of the PAA at 1.45 GHz

Parameters	*conf*-16	*conf*-3	*conf*-7	*conf*-12	Units
peak gain	4.95	4.82	4.82	5.08	dBi
main lobe direction	0	115	180	290	°
HPBW	79	80	69	91	°
FB ratio	22.7	17.5	16.7	19.4	dB

The lower values in the peak gain can be explained by higher argon pressure values that are due to the uncertainty in the pressure measurement process; an increase in the neutral gas pressure leads to an increase in the collision frequency (see (1)), that in turn leads to higher losses within the plasma discharge and, ultimately, a decrease in the gain. In addition, the uncertainty in the interferometer measurement can justify lower values of the plasma density within the discharge, that along with the unwanted density

Table 3 Numerically calculated peak gain, main lobe direction, HPBW, and FB ratio of the PAA at 1.45 GHz

Parameters	*conf*-16	*conf*-3	*conf*-7	*conf*-12	Units
peak gain	7.85	6.95	5.48	7.36	dBi
main lobe direction	0	85	180	290	°
HPBW	92	98	80	93	°
FB ratio	17.9	18.3	22.5	17.9	dB

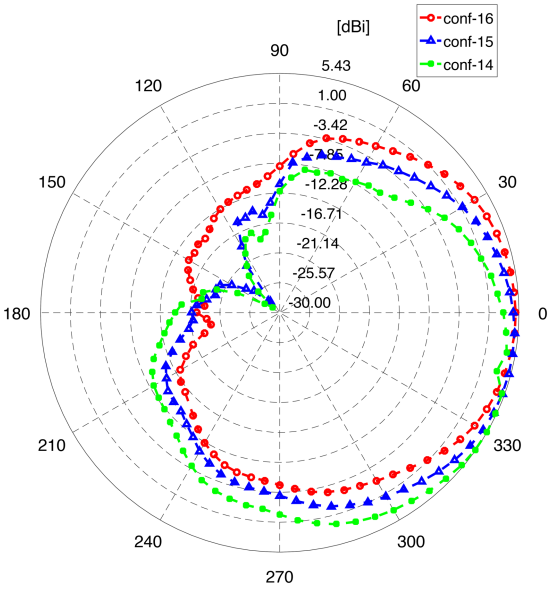

Fig. 12 *Gain pattern (g(θ) in dBi) on the H-plane at 1.45 GHz from measurement in the anechoic chamber of the plasma array antenna configurations: conf-16, conf-15, and conf-14 (see Table 1 for table of configurations). θ angles are measured from x-axis to y-axis (see Fig. 1)*

profile can justify a suboptimal reflecting behaviour of the plasma discharges. This reasoning along with the above-mentioned complexity of the antenna set-up, which has not been considered in the numerical model (see Fig. 1), can explain the discrepancy in the gain pattern shape and consequently in the HPBW, the FB ratio, and the main lobe direction values between the numerical and experimental results.

Similar considerations hold true for all the configurations *conf-2* through to *conf-19* (see Table 1 for reference) that realise beam-forming operations of the antenna. Regarding the remaining configurations, numerical simulations point out an omnidirectional gain pattern of both *conf*-1 and *conf*-20 with a gain value of 1.24 and −8 dB, respectively; therefore, plasma discharges in *conf*-20 act as a sort of shield that attenuates incoming radiation.

To verify the minimal angular step in steering the radiation pattern, we have considered the antenna configurations *conf*-14, *conf*-15, and *conf*-16 (see Table 1 for table of configurations), that are expected to tilt the main lobe towards 320°, 340°, and 360°, respectively. In Fig. 12, we report the gain pattern of the three configurations that were obtained from the anechoic chamber; the results show that the tilt angles are 330°, 345°, and 360°, respectively, with the peak gain values of 5.12, 5.43, and 4.95 dBi, respectively. Similarly, the discrepancy between the measured and expected main lobe directions is due to the suboptimal reflection behaviour of the plasma discharges, and the complexity of the antenna set-up.

5 Conclusion

In this work, we have designed, fabricated, and tested a plasma reflector antenna that allows to electronically reconfigure the radiation pattern of a conventional dipole that works in the Galileo navigation frequency band. The antenna prototype features customised plasma discharge tubes that have been filled with argon at a certain pressure and the plasma density has been measured by a microwave interferometer; this approach allows to determine the plasma electric permittivity, which has been used in the numerical model.

The magnitude of the reflection coefficient and the gain pattern on the *H*-plane of the analysed configurations exhibit a satisfactory agreement between numerical and experimental results. These results confirm that the central omnidirectional antenna can provide beam-forming capabilities by controlling the subset of ignited plasma discharges.

6 Acknowledgment

This work was supported by the Italian Space Agency (grant no. 2015-030-I.0).

7 References

[1] Alexeff, I., Anderson, T., Parameswaran, S., *et al.*: 'Experimental and theoretical results with plasma antennas', *IEEE Trans. Plasma Sci.*, 2006, **34**, (2), pp. 166–172
[2] Anderson, T.: '*Plasma antennas*' (Artech House, Norwood, MA, 2011)
[3] Melazzi, D., Lancellotti, V., Capobianco, A.D.: 'Analytical and numerical study of a gaseous plasma dipole in the UHF frequency band', *IEEE Trans. Antennas Propag.*, 2017, **65**, (12), pp. 7091–7101
[4] Borg, G., Harris, J., Miljak, D., *et al.*: 'Application of plasma columns to radiofrequency antennas', *Appl. Phys. Lett.*, 1999, **74**, (22), pp. 3272–3274
[5] Borg, G., Harris, J., Martin, N., *et al.*: 'Plasmas as antennas: theory, experiment and applications', *Phys. Plasmas*, 2000, **7**, (5), pp. 2198–2202
[6] Anderson, T., Alexeff, I., Farshi, E., *et al.*: 'An operating intelligent plasma antenna'. 16th IEEE Int. Pulsed Power Conf., Albuquerque, NM, 2007
[7] Chen, F.F.: '*Introduction to plasma physics and controlled fusion. Volume 1: plasma physics*' (Plenum Press, New York, 1984, 2nd edn.)
[8] Fernandez-Olver, A.D.J., Melazzi, D., Lancellotti, V.: 'Beam-forming and beam-steering capabilities of a reconfigurable plasma antenna array', *Prog. Electromagn. Res. C*, 2016, **65**, pp. 11–22
[9] Wu, X.P., Shi, J.M., Chen, Z.S., *et al.*: 'A new plasma antenna of beam-forming', *Prog. Electromagn. Res. C*, 2012, **126**, pp. 539–553
[10] Zhu, A., Chen, Z., Lv, J.: 'Reconfigurable characteristics of the monopole plasma antenna and its array driven by surface wave', *WSEAS Trans. Commun.*, 2013, **12**, (4), pp. 143–153
[11] Malhat, H.A., Badawy, M.M., Zainud-Deen, S.H., *et al.*: 'Dual-mode plasma reflectarray/transmitarray antennas', *IEEE Trans. Plasma Sci.*, 2015, **43**, (10), pp. 3582–3589
[12] Dwyer, T., Greg, J., Murphy, D., *et al.*: 'On the feasibility study of using an atmospheric discharge plasma as an RF antenna', *IEEE Trans. Antennas Propag.*, 1984, **32**, pp. 141–146
[13] Lieberman, M., Lichtenberg, A.: '*Principles of plasma discharges and materials processing*' (John Wiley & Sons, Inc., Hoboken, NJ, 2005, 2nd edn.)
[14] Moisan, M., Shivarova, A., Trivelpiece, A.: 'Experimental investigations of the propagation of surface waves along a plasma column', *Phys. Plasmas*, 1982, **24**, p. 1331
[15] Robson, A., Morgan, R., Meger, R.A.: 'Demonstration of a plasma mirror for microwaves', *IEEE Trans. Plasma Sci.*, 1992, **32**, (6), pp. 1036–1040
[16] Meger, R.A., Mathew, J., Gregor, J.A., *et al.*: 'Experimental investigations of the formation of a plasma mirror for high-frequency microwave beam steering', *Phys. Plasmas*, 1995, **2**, p. 2532
[17] Bliokh, Y.P., Felsteiner, J., Slutsker, Y.Z.: 'Plasma generation for controlled microwave-reflecting surfaces in plasma antennas', *J. Appl. Phys.*, 2014, **115**, p. 163305
[18] Ja'afar, H, Ali, M.T.B., Dagang, A.N.B., *et al.*: 'A reconfigurable monopole antenna with fluorescent tubes using plasma windowing concepts for 4.9-GHz application', *IEEE Trans. Plasma Sci.*, 2015, **43**, (3), pp. 815–820
[19] Yamamoto, T., Kobayashi, T.: 'A reconfigurable antenna using fluorescent lamps'. Int. Symp. Antennas and Propagation, Kaohsiung, Taiwan, 2–5 December, 2014
[20] Jusoh, M.T., Lafond, O., Colombel, F., *et al.*: 'Performance and radiation patterns of a reconfigurable plasma corner-reflector antenna', *IEEE Antennas Wirel. Propag. Lett.*, 2013, **99**, p. 1
[21] Melazzi, D., Lancellotti, V.: 'ADAMANT: 'a surface and volume integral-equation solver for the analysis and design of helicon plasma sources', *Comput. Phys. Commun.*, 2014, **185**, pp. 1914–1925
[22] Balanis, C.A.: 'Reflector antennas', in Balanis, C.A. (Ed.): '*Antenna theory: analysis and design*' (Wiley, Hoboken, NJ, USA, 2005, 3rd edn.), pp. 883–892
[23] Swanson, D.G.: '*Plasma waves*' (Institute of Physics Publishing, Boca Raton, FL, 2003, 2nd edn.)
[24] Tudisco, O., Lucca Fabris, A., Falcetta, C., *et al.*: 'A microwave interferometer for small and tenuous plasma density measurements', *Rev. Sci. Instrum.*, 2013, **84**, p. 033505